Osaka University
Theoretical Astrophysics

OU-TAP 64
YITP-97-41

February 7, 2008

Numerical study on the hydrodynamic instability of binary stars in the first post Newtonian approximation of general relativity

arXiv:gr-qc/9710023v1 3 Oct 1997

Masaru Shibata, Ken-ichi Oohara[†], and Takashi Nakamura[*]

Department of Earth and Space Science, Graduate School of Science, Osaka University, Toyonaka, Osaka 560, Japan

[†]*Department of Physics, Niigata University, Niigata 950-21, Japan*

[*]*Yukawa Institute for Theoretical Physics, Kyoto University, Kyoto 606-01, Japan*

Abstract

We present numerical results on the hydrodynamic stability of coalescing binary stars in the first post Newtonian(1PN) approximation of general relativity. We pay particular attention to the hydrodynamical instability of corotating binary stars in equilibrium states assuming the stiff polytropic equation of state with the adiabatic constant $\Gamma = 3$. In previous 1PN numerical studies on corotating binary stars in equilibrium states, it was found that along the sequence of binary stars as a function of the orbital separation, they have the energy and/or angular momentum minima where the secular instability sets in, and that with increase of the 1PN correction, the orbital separation at these minima decreases while the angular velocity there increases. In this paper, to know the location of the innermost stable circular orbit(ISCO), we perform numerical simulations and find where the hydrodynamical instability along the corotating sequences of binary sets in. From the numerical results, we found that the dynamical stability limit seems to exist near the energy and/or angular momentum minima not only in the Newtonian, but also in the 1PN cases. This means that the 1PN effect of general relativity increases the angular frequency of gravitational waves at the ISCO.

§1. Introduction

The laser interferometric gravitational wave detectors such as LIGO [1], VIRGO [2], GEO600 [3] and TAMA300 [4] will be in operation within four years or so. One of the most important astrophysical sources of gravitational waves for these detectors is coalescing binary neutron stars(BNS's) because gravitational waves emitted in the late inspiraling phase have frequencies in the sensitive region of these detectors, i.e., from 10Hz to 1000Hz. We will be able to know each mass and spin of BNS's if we can obtain an accurate theoretical template for data analysis [5]. For that reason, much theoretical effort has been paid to obtain a theoretical template as accurate as possible [6].

When the orbital separation of BNS's becomes a few times of the neutron star(NS) radius, the hydrodynamical effect becomes important. In such a post inspiraling phase, the wave form of gravitational waves is expected to be sensitive to the structure of NS such as the relation between the radius and the mass of NS. Thus, if gravitational waves from such a phase are detected, we may constrain the equation of state(EOS) of NS [7] [8] [9]. In particular, it is important to know the innermost stable circular orbit(ISCO), where the binary will change the orbit from the stable inspiraling orbit to the merging one. Since its location will be sensitive to the structure of NS, it will bring us an important information on the EOS of NS.

The location of the ISCO is determined both by (1) the pure general relativistic(GR) effect on two spherical bodies and by (2) the hydrodynamical effect. Recently, Lai, Rasio and Shapiro(LRS) pointed out the importance of the latter effect [9]: They showed that when the orbital separation of BNS's becomes sufficiently small, but larger than the approximate radius of the ISCO for two spherical bodies $\sim 6GM/c^2$ where M is the total mass of the system, each star of binary is significantly deformed by the tidal force from the companion star. Then, an additional tidal field due to the deformation of each star is generated and as a result, the circular orbit of BNS's becomes hydrodynamically unstable before two stars come into contact even in the Newtonian case if the EOS of NS is stiff enough.

Such a tidal effect will be sensitive to the structure of NS because the degree of the tidal deformation depends on it. Since general relativity plays an important role in determining the structure of NS, we can expect that this is also the case in determining the location where the hydrodynamical stability due to the tidal force sets in. To know the effect of general relativity, as a first step, Shibata [10] [11] numerically obtained the equilibrium state of corotating binary of equal mass in the 1PN approximation and investigated the stability of such binaries. The purpose of his works was to clarify the 1PN effect of general relativity in BNS's. The main conclusions he obtained are (a) along the equilibrium sequence, there

exist the energy and/or angular momentum minima where the secular instability of binary sets in [9], and (b) the orbital separation at the minima decreases due to 1PN correction, and as a result, the orbital angular velocity there increases.

As LRS showed for the Newtonian case, the secular instability limit does not coincide with the dynamical one for corotating binary, and the orbital separation of the latter one will locate slightly inside the former one [9]. The ISCO is defined as the dynamical instability limit, which is found only by performing numerical simulation. Hence, in order to determine the dynamical instability limit along the sequence of corotating binary, we should perform numerical simulations and judge the dynamical stability. In this paper we will show that the hydrodynamical instability occurs near the energy and/or angular momentum minima not only in the Newtonian cases but also in the 1PN cases.

This paper is organized as follows. In §2, we show the 1PN hydrodynamic equations to be solved which are slightly different from previous ones [12]: In particular, we change the form of the energy equation. In §3, we briefly describe the method for numerical simulation. In §4, numerical results are shown: In this paper, we pay attention to binaries of the polytropic EOS of the adiabatic index $\Gamma = 3$ for which the energy and angular momentum minima for equilibrium sequences were clearly obtained for both the Newtonian and 1PN cases in previous papers [10) 11)]. We show numerical results and discuss the dynamical stability of binaries around those minima. §5 is devoted to summary. Throughout this paper, G, c, and $M_\odot$ denotes the gravitational constant, the speed of light and the solar mass.

§2. Basic equations

In the 1PN approximation with the standard gauge condition, the line element is written as [13]

$$ds^2 = g_{\mu\nu}dx^\mu dx^\nu = -\alpha^2 c^2 dt^2 + \frac{2}{c^2}\beta_i dx^i dt + \psi^4 \tilde{\gamma}_{ij} dx^i dx^j$$

where

$$\alpha = 1 - \frac{U_*}{c^2} + \frac{1}{c^4}\left(\frac{U_*^2}{2} + X_*\right) + O(c^{-6}), \tag{2·1}$$

$$\psi = 1 + \frac{U_*}{2c^2} + O(c^{-4}), \tag{2·2}$$

$$\tilde{\gamma}_{ij} = \delta_{ij} + O(c^{-4}). \tag{2·3}$$

Here, β_i is calculated from

$$\beta_i = -\frac{7}{2}P_{*i} + \frac{1}{2}\left(x^j P_{*j,i} + \chi_{,i}\right). \tag{2·4}$$

Equations for gravitational potentials, U_*, X_*, P_{*i} and χ, are shown below.

The energy-momentum tensor is

$$T^{\mu\nu} = \rho\left(c^2 + \varepsilon + \frac{P}{\rho}\right)u^\mu u^\nu + Pg^{\mu\nu}, \tag{2·5}$$

where ρ, ε, P and u^μ are the baryon density, the internal energy, the pressure, and the four velocity, respectively. In the 1PN approximation, components of four velocity are written as

$$u^0 = 1 + \frac{1}{c^2}\left\{\frac{1}{2}v^2 + U_*\right\} + O(c^{-4}), \tag{2·6}$$

$$u_0 = -\left[1 + \frac{1}{c^2}\left\{\frac{1}{2}v^2 - U_*\right\} + O(c^{-4})\right], \tag{2·7}$$

$$u^i = \frac{v^i}{c}\left[1 + \frac{1}{c^2}\left\{\frac{1}{2}v^2 + U_*\right\} + O(c^{-4})\right], \tag{2·8}$$

$$u_i = \frac{v^i}{c} + \frac{1}{c^3}\left\{\beta_i + v^i\left(\frac{v^2}{2} + 3U_*\right)\right\} + O(c^{-5}), \tag{2·9}$$

where

$$v^i = \frac{u^i}{u^0} \quad \text{and} \quad v^2 = v^i v^i. \tag{2·10}$$

As the EOS, we assume the polytropic one as

$$P = (\Gamma - 1)\rho\varepsilon. \tag{2·11}$$

The continuity equation is

$$\nabla_\mu(\rho u^\mu) = 0\ . \tag{2·12}$$

Using the variable $\rho_* = \rho\alpha u^0\psi^6$, we rewrite the continuity equation as

$$\frac{\partial\rho_*}{\partial t} + \frac{\partial(\rho_* v^i)}{\partial x^i} = 0\ . \tag{2·13}$$

In the 1PN approximation, ρ_* is

$$\rho_* = \rho\left\{1 + \frac{1}{c^2}\left(\frac{v^2}{2} + 3U_*\right) + O(c^{-4})\right\}. \tag{2·14}$$

From the conservation of the energy momentum tensor,

$$\begin{aligned}\nabla_\mu T^\mu_{\ \nu} =& \frac{1}{\alpha\psi^6}\frac{\partial}{\partial x^\mu}\left\{\alpha\psi^6\left(\rho c^2 + \rho\varepsilon + P\right)u^\mu u_\nu\right\} \\ & -\frac{1}{2}\left(\rho c^2 + \rho\varepsilon + P\right)u^\mu u^\sigma g_{\mu\sigma,\nu} + P_{,\nu} \\ =& 0,\end{aligned} \tag{2·15}$$

we obtain eqautions for the Euler and the entropy conservation as

$$\frac{\partial(\rho_*\hat{u}_i)}{\partial t}+\frac{\partial(\rho_*\hat{u}_i v^j)}{\partial x^j}=-\alpha\psi^6 P_{,i}-\rho_*\alpha\hat{u}^0\alpha_{,i}+\rho_*\hat{u}_j\beta^j{}_{,i}-\frac{\rho_*}{2\hat{u}^0}\hat{u}_j\hat{u}_k\gamma^{jk}{}_{,i} \tag{2·16}$$

$$\frac{\partial e_*}{\partial t}+\frac{\partial(e_* v^j)}{\partial x^j}=0, \tag{2·17}$$

where

$$\hat{u}_i\equiv\left\{1+\frac{1}{c^2}\left(\varepsilon+\frac{P}{\rho}\right)\right\}u_i, \tag{2·18}$$

$$\hat{u}^0\equiv\left\{1+\frac{1}{c^2}\left(\varepsilon+\frac{P}{\rho}\right)\right\}u^0, \tag{2·19}$$

$$e_*\equiv(\rho\varepsilon)^{1/\Gamma}\alpha u^0\psi^6. \tag{2·20}$$

In the 1PN approximation, the Euler equation becomes

$$\frac{\partial(\rho_*\hat{u}_i)}{\partial t}+\frac{\partial(\rho_*\hat{u}_i v^j)}{\partial x^j}=-\left(1+\frac{2U_*}{c^2}\right)P_{,i}+\rho_*\left[\left\{1+\frac{1}{c^2}\left(\varepsilon+\frac{P}{\rho}+\frac{3v^2}{2}-U_*\right)\right\}U_{*,i}-\frac{X_{*,i}}{c^2}+\frac{v^j\beta_{j,i}}{c^2}\right]+O(c^{-4})\ , \tag{2·21}$$

where

$$\hat{u}_i=v^i\left\{1+\frac{1}{c^2}\left(\varepsilon+\frac{P}{\rho}+\frac{v^2}{2}+3U_*\right)\right\}+\frac{\beta_i}{c^2}+O(c^{-4})\ . \tag{2·22}$$

The pressure is calculated from

$$P=(\Gamma-1)e_*^{\Gamma}\left\{1+\frac{1}{c^2}\left(\frac{v^2}{2}+3U_*\right)\right\}^{-\Gamma}. \tag{2·23}$$

We notice that the form of the 1PN hydrodynamic equations, in particular the entropy equation, shown above are different from those of Blanchet, Damour, and Schäfer [12] although in both formalisms, every 1PN term is taken into account consistently. Thus, equations adopted in this paper are different from those used in a previous paper [14].

Equations for various potentials U_*, X_*, P_{*i} and χ are derived from the Einstein equation as

$$\Delta U_*=-4\pi G\rho_*, \tag{2·24}$$

$$\Delta P_{*i}=-4\pi G\rho_* v^i, \tag{2·25}$$

$$\Delta X_*=4\pi G\rho_*\left(\frac{3v^2}{2}-U_*+\varepsilon+\frac{3P}{\rho}\right), \tag{2·26}$$

$$\Delta\chi=4\pi G\rho_* v^i x^i. \tag{2·27}$$

Note that the definitions of the gravitational potentials are based on ρ_*, not on ρ. Thus, they are different quantities from those defined in obtaining the equilibrium state [10) 11)] in which we need to use the gravitational potentials defined with respect to ρ. (For example, the Newtonian potential U which satisfies $\Delta U = -4\pi\rho$ differs from U_*.)

We use the following forms of the continuity, Euler, and the entropy equations as the basic equations in the Newtonian case:

$$\frac{\partial \rho}{\partial t} + \frac{\partial (\rho v^j)}{\partial x^j} = 0, \tag{2·28}$$

$$\frac{\partial (\rho v^i)}{\partial t} + \frac{\partial (\rho v^i v^j)}{\partial x^j} = -\frac{\partial P}{\partial x^i} + \rho \frac{\partial U}{\partial x^i}, \tag{2·29}$$

$$\frac{\partial e}{\partial t} + \frac{\partial (e v^j)}{\partial x^j} = 0, \tag{2·30}$$

where $e = (\rho\varepsilon)^{1/\Gamma} = [P/(\Gamma - 1)]^{1/\Gamma}$. Thus, we change the form of the energy equation from that adopted in previous papers [15) 16)]. We emphasize that this choice improves accuracy on the conservation of the energy and angular momentum in numerical simulation compared with our previous works.

Before closing this section, we define the following quantities correct up to 1PN order:

- Conserved mass and Newtonian mass

$$M_* = \int \rho_* dV \qquad \text{and} \qquad M = \int \rho dV. \tag{2·31}$$

  Note that for the Newtonian case, $M_* = M$.

- The energy: In the definition based on ρ,

$$E = \int \rho \left\{ \varepsilon + \frac{v^2}{2} - \frac{1}{2}U + \frac{1}{c^2}\left(\frac{5}{8}v^4 + \frac{5}{2}v^2 U + \frac{1}{2}\beta_i v^i + \varepsilon v^2 + \frac{P}{\rho}v^2 \right.\right.$$
$$\left.\left. + 2\varepsilon U - \frac{5}{2}U^2 \right) \right\} dV, \tag{2·32}$$

  while in the definition based on ρ_*,

$$E = \int \rho_* \left\{ \varepsilon + \frac{v^2}{2} - \frac{1}{2}U_* + \frac{1}{c^2}\left(\frac{3}{8}v^4 + \frac{3}{2}v^2 U_* + \frac{1}{2}\beta_i v^i + \frac{1}{2}\varepsilon v^2 + \frac{P}{\rho}v^2 \right.\right.$$
$$\left.\left. - \varepsilon U_* + \frac{1}{2}U_*^2 \right) \right\} dV$$
$$\equiv E_*. \tag{2·33}$$

- The angular momentum around the rotation axis : In the definition based on ρ,

$$J = \int \rho \left[(-yv^x + xv^y) \left\{ 1 + \frac{1}{c^2} \left(v^2 + 6U + \varepsilon + \frac{P}{\rho} \right) \right\} + \frac{1}{c^2}(-y\beta_x + x\beta_y) \right] dV, \quad (2\cdot34)$$

while in the definition based on ρ_*,

$$J = \int \rho_* (-y\hat{u}_x + x\hat{u}_y) dV \equiv J_*. \quad (2\cdot35)$$

Note that we adopt the z-axis as the rotation axis in this paper. Here, we also notice that numerical values E and E_* or J and J_* are, respectively, slightly and systematically different because some terms of $O(c^{-4})$ are implicitly included in E_* and J_*. However, the difference is small and not important in the following discussions. In the following, we use J_* as the angular momentum in numerical simulations, while we use the definition based on ρ as the angular momentum of the equilibrium sequence.

- Center of mass of each star

$$x_g^i = \frac{1}{M_*} \int_{\text{each star}} \rho_* x^i dV. \quad (2\cdot36)$$

From x_g^i, we define the coordinate separation of the orbital radius as $r_g = 2(x_g^i x_g^i)^{1/2}$.

- The quadrupole moment of system

$$I_{ij} = \int \rho_* x^i x^j dV. \quad (2\cdot37)$$

We also define

$$I_{RR} \equiv I_{xx} + I_{yy}, \qquad \text{and} \qquad \tilde{I}_{ij} = I_{ij} - \frac{1}{3}\delta_{ij} I_{kk}, \quad (2\cdot38)$$

where δ_{ij} is the Kronecker's delta.

§3. Numerical method

In numerical computation, we solve (1) the 1PN hydrodynamic equations and (2) the Poisson equations for various potentials. In the following, we mention the numerical methods we adopt briefly.

Our treatment for the advection term in the hydrodynamic equations is the same as that adopted in previous papers [15) 14) 16)]. Although the method is the same, the energy equation we adopt is different from the previous one. As a result, accuracy on the conservation of the angular momentum and the energy of the system is significantly improved.*) As for the

*) We here note that using the entropy equation adopted above, the entropy is conserved. If the shock is formed, however, the entropy should not be conserved. Hence, we must introduce the artificial viscosity term in the Euler and entropy equations to express the shock accurately. In this paper, however, the shock formation does not play an important role, so that we do not add such terms.

time evolution, we use the second order Runge-Kutta method. Thus, the numerical code for solving the hydrodynamic equations is second order accurate both in time and space. (Actually, we checked, for example, that accuracy of the conservation of the total energy is second order convergent changing the grid number.)

Since we use the stiff EOS, density near the surface of each star decreases steeply. With a finite resolution of numerical grid, one cannot accurately represent the density decline near the surface. As a result, the pressure gradient often happens to become too steep, and the velocity near the surface becomes unphysically too large. To avoid that, when the density ρ_* is less than $\rho_{\rm crit} \simeq 2 \times 10^{-4} \rho_{\rm max}$, where $\rho_{\rm max}$ is the maximum of ρ_*, we artificially suppress the linear momentum $\hat{u}_i$(or v^i for the Newtonian case) near the surface by a factor $\rho_*/(\rho_* + f\rho_{\rm max})$, where f is a small factor and we set as $\simeq 4 \times 10^{-5}$. This technique has been used in our series of papers [15) 14) 16)].

To solve 6 Poisson equations for U_*, X_*, P_{*x}, P_{*y}, P_{*z}, and χ, we use the ICCG method as we have done in previous papers [15) 14) 16)] imposing the boundary conditions at outer grids as

$$U_* \to \frac{GM_*}{r} + O(r^{-3}), \tag{3·1}$$

$$X_* \to -\frac{G}{r}\int \rho_* \left(\frac{3v^2}{2} - U_* + \varepsilon + \frac{P}{\rho} \right) dV + O(r^{-3}), \tag{3·2}$$

$$P_{*x} \to \frac{Gx}{r^3}\int \rho_* x v^x dV + \frac{Gy}{r^3}\int \rho_* y v^x dV + O(r^{-4}), \tag{3·3}$$

$$P_{*y} \to \frac{Gx}{r^3}\int \rho_* x v^y dV + \frac{Gy}{r^3}\int \rho_* y v^y dV + O(r^{-4}), \tag{3·4}$$

$$P_{*z} \to \frac{Gz}{r^3}\int \rho_* z v^z dV + O(r^{-4}), \tag{3·5}$$

$$\chi \to -\frac{G}{r}\int \rho_* v^i x^i dV + O(r^{-3}). \tag{3·6}$$

Thus, we use three types of numerical implementations for solving Poisson equations for (U_*, X_*, χ), (P_{*x}, P_{*y}), and P_{*z}, respectively. Accuracy of these Poisson solvers has been checked to be less than 0.1% and a result for the case of a small grid number is shown in [17)].

Throughout this paper, we assume the symmetry with respect to the equatorial plane. Thus, we also impose boundary conditions at the equatorial plane as

$$\begin{aligned} &\rho_*(-z) = \rho_*(z), \quad e_*(-z) = e_*(z), \quad v^A(-z) = v^A(z), \\ &v^z(-z) = -v^z(z), \quad U_*(-z) = U_*(z), \quad X_*(-z) = X_*(z), \\ &\chi(-z) = \chi(z), \quad P_{*A}(-z) = P_{*A}(z), \quad P_{*z}(-z) = -P_{*z}(z), \end{aligned} \tag{3·7}$$

where $A = x$ or y. Grid number we adopt is $(N_x, N_y, N_z) = (141, 141, 71)$, and grid spacing is chosen in order that the grid covers the minor axis of each star at initial state by at

least 15 grid points. Numerical computations were performed on FACOM VX4 in the data processing center of National Astronomical Observatory in Japan.

FACOM VX4 has four parallel processors, so that four different procedures can be done on separate processors at the same time. To solve the Poisson equations in the 1PN case, we make use of this property: In each time step, we solve the Poisson equations for U_* and X_* on processor 1, for P_{*x} and P_{*y} on processor 2, for P_{*z} on processor 3, and for χ on processor 4, while the hydrodynamic equations are solved only on processor 1. Since computation of solving the Poisson equations is the most time-consuming part in the numerical implementations, the CPU time required reduces by a factor of ~ 3 in the 1PN case using this simple technique. On the other hand, we only use one processor in the Newtonian case because only one Poisson equation is required to be solved. In a typical computation for one model, $20000 \sim 30000$ time steps were necessary, and computation of 20000 time steps took about 30 CPU hours for the Newtonian case, and about 65 CPU hours for the 1PN case.

§4. Numerical results

We assume $\Gamma = 3$ as the adiabatic index because we are interested in BNS's which are composed of a stiff EOS, i.e., $\Gamma = 2 \sim 3$ [18]. As initial conditions of binary, we adopt equilibrium states of binary corotating around the z-axis. When we obtain such a solution, we set the EOS as

$$P = K\rho^{\Gamma}, \tag{4·1}$$

where K is the polytropic constant. Following a previous paper [10], for convenience, we set K as

$$K = 2.524 G r_0^5 M_\odot^{-1}. \tag{4·2}$$

Then, the radius of each star of binary in the Newtonian limit is $r_0(M/M_\odot)^{0.2} \equiv a_0$. In the following, M_* denotes the conserved mass of each star of binary and is set as $1.4M_\odot$. In this paper, we consider two cases, the Newtonian case(i.e., $c \to \infty$ in the PN approximation) and the 1PN case of $r_0 = 40R_s$ where $R_s = GM_\odot/c^2$. We note that for $r_0 = 40R_s$, the compactness of each star is $C_{\rm s} \equiv GM_*/a_*c^2 \simeq 0.033$, where $a_* \equiv r_0(M_*/M_\odot)^{0.2}$(note that $a_* = a_0$ in the Newtonian case), and this value is too small to represent realistic BNS's which we are most interested in. However, the PN approximation is valid only for weak gravity, i.e., for small compactness, and it is meaningless to apply it for large compactness. We emphasize that the main aim of this paper is to solidly know the 1PN effect which will play an important role in BNS's.

In figs.1, we show the energy and the angular momentum of corotating binary in equilibrium states as a function of the orbital separation r_g/a_* for the 1PN case of $r_0 = 40R_s$(filled circles) and the Newtonian case(open circles). As shown in previous papers [10) 11)], there exist the minima along the sequences of the energy and angular momentum, and the separation at the minima becomes small with increase of the 1PN effect: For the Newtonian case, the separation is $r_g \simeq 3.08a_0$, and for the 1PN case of $r_0 = 40R_s$, it is $r_g \simeq 2.94a_*$.

We will perform numerical simulations using some of such equilibrium states near the energy and/or angular momentum minima as initial conditions. Among equilibrium states along each sequence, we choose four states as initial conditions: they are N5, N6, N7, and N8 along the Newtonian sequence, and PN5, PN6, PN7, and PN8 along the 1PN sequence, respectively. Models N6 and PN6 are equilibrium states at the nearest location from the energy and/or angular momentum minima.

In figs.2(a) and (b), we show the evolution of I_{RR} for the Newtonian and 1PN cases, respectively. Hereafter, we use the unit of time as $4\pi\sqrt{a_*^3/GM_*}$, and in this unit, the orbital periods of equilibrium states are $\simeq 1.82$ for N5, 1.88 for N6, 1.95 for N7, 2.03 for N8, 1.74 for PN5, 1.80 for PN6, 1.87 for PN7, 1.95 for PN8, respectively. On the other hand, the vertical axis is shown in units of $M_*a_*^2$(i.e., $I = I_{RR}/(M_*a_*^2)$). This means that when $I \lesssim 2$, the binary begins to merge. Hereafter, solid, dotted, dashed and dotted-dashed lines are used to show quantities for models N5(PN5), N6(PN6), N7(PN7), and N8(PN8), respectively.

Figs.2 show that equilibrium models N5, N6, PN5 and PN6 seem hydrodynamically unstable; two stars merge within about one orbital period. On the other hand, models N7, N8, PN7, and PN8 seem hydrodynamically stable because in these binaries, two stars do not come into merging in the dynamical time scale(i.e., the orbital period). We note that irrespective of the hydrodynamical stability, the orbit of binaries shrinks due to dissipation of the angular momentum. This occurs because of a finite resolution(i.e., finite accuracy) both in time and space in the numerical simulation, and is the reason why I decreases gradually for stable binaries such as N7, N8, PN7, and PN8.

In fig.3, we show the angular momentum as a function of time for the Newtonian and 1PN cases(note that for the 1PN case, the angular momentum is J_*). Here, the unit of the angular momentum is $G^{1/2}M_*^{3/2}a_*^{1/2}$, and the unit of the time is the same as that in figs.2. Notice that a small fraction of matter carrying the large angular momentum is ejected outside the numerical grids in model PN5 for $t \gtrsim 2.6$, and in model N5 for $t \gtrsim 2.9$ so that the angular momentum is decreasing. Fig.3 shows that accuracy on the conservation of the angular momentum is fairly good in all simulations, but it is not perfect: In one orbital period, the angular momentum is lost by about $\sim 0.1\%$.

Even for the angular momentum loss, equilibrium models N7, N8, PN7, and PN8 do

not proceed to merging in the dynamical time scale. Thus, these binaries seem obviously stable. On the other hand, we cannot completely deny the possibility that a small loss of the angular momentum by such numerical effects leads models N5, N6, PN5 and PN6 to unstable orbits. However, the loss of the angular momentum is not so large up to the contact of these binaries. According to an approximate analysis by LRS(see, for example, fig.1 in [9]), the hydrodynamically stable corotating binary will move to another stable binary which is not corotating state even when it slightly loses the angular momentum(unless its loss is so large). Hence, we judge that the hydrodynamical instability will really occur when the orbital separation of binary becomes as small as that of N5, N6, PN5 and PN6 or slightly smaller than these, i.e. very near or slightly inside the energy and/or angular momentum minima along the sequences of corotating binaries, $r_g \sim 3.08a_0$ for the Newtonian case, and $r_g \sim 2.94a_*$ for the 1PN case of $C_{\rm s} \simeq 0.033$.

We note the following fact: As for the Newtonian study on the determination of the dynamically stability limit for the $\Gamma = 3$ case, there have been two independent works by Rasio and Shapiro(RS) [19] and New and Tohline(NT) [20], and their results slightly disagree: According to RS, the dynamical instability along the corotating sequence sets in at $r_g \simeq 2.97a_0$, while according to NT, it sets in at $r_g \simeq 3.08a_0$. The hydrodynamic code which RS used in their numerical simulations is a SPH one, while that used by NT is the Eulerian one. In our present simulation, we use the Eulerian code, and this may be the reason why the present results support the work by NT. Currently, however, the reason for this slight difference is not clear.

In fig.4, we show the maximum density of the system as a function of time for the Newtonian and 1PN cases, respectively. The density is shown in units of $M_*(4\pi a_*^3/3)^{-1}$. Fig.4 shows that apart from a small oscillation, the maximum density is almost constant for the case where two stars of the binary do not merge. We notice that the maximum density for the 1PN configuration are larger than that for the Newtonian one for a given angular frequency. This is a manifestation of the GR effect by which each star of binary is forced to be more compact than that in the Newtonian case. It should be also noted that along not only the Newtonian equilibrium sequence, but also the 1PN one, the central density decreases with decrease of the orbital separation [21) 22)].

In figs.5 and 6, we show the evolution of the density profile in the equatorial plane for models N7 and PN7. Note that x- and y-axes are shown in units of a_*, outermost grid is placed at 4.09 in this unit, and the orbital rotation is counterclockwise. Figs.5 and 6 show that for more than one orbital period, the density profile does not change so much apart from a small deformation in the outer region of each star. Thus, in our present numerical simulation, the density profile of equilibrium state can be kept fairly well for

hydrodynamically stable models.

In figs.7 and 8, we show the evolution of the density profile in the equatorial plane for models N5 and PN5, i.e., dynamically unstable models, respectively. In both Newtonian and 1PN cases, the evolution is similar to that obtained by RS [19]: In about one orbital period, two stars merge due to the hydrodynamic instability. After they merge, spiral arms are formed and they transport the angular momentum outward. In the final stage, the spiral arms widen and merge together. In the central region, an ellipsoidal core is formed. Since radiation reaction of gravitational waves is not taken into account in this paper, the ellipsoidal figure will be kept forever.

Finally, we show the wave form and the luminosity of gravitational waves for merging phase of binary. Although we are able to calculate the 1PN wave form and luminosity using the Blanchet, Damour, and Schäfer formalism [12], in this paper we simply show the Newtonian ones. In figs.9(a) and (b), we show + and × modes of gravitational waves observed along the z-axis for models PN5(solid lines) and N5(dotted lines). + and × modes are defined as

$$r_o h_+ = \frac{G}{c^4}\frac{d^2}{dt^2}\left(I_{xx} - I_{yy}\right), \qquad \text{and} \qquad r_o h_\times = \frac{2G}{c^4}\frac{d^2}{dt^2} I_{xy}, \tag{4·3}$$

where r_o denotes the distance from the source to an observer on the z-axis. In fig.9(c), we show the luminosity defined as

$$\frac{dE}{dt} = \frac{G}{5c^5}\frac{d^3 \mathcal{I}_{ij}}{dt^3}\frac{d^3 \mathcal{I}_{ij}}{dt^3}. \tag{4·4}$$

Since the orbital period of model PN5 is shorter than that of N5, the wave length of gravitational waves before merging for PN5 is shorter than that of N5. Also, the each star of model PN5 is more compact than that of N5, so that the maximum amplitude of the luminosity for PN5 is larger than that for N5. Although these differences exist between PN and Newtonian results, overall shapes of the wave form and luminosity in the PN approximation are essentially the same as those in the Newtonian case(see also figs.10 and 11 in ref. [19]): As the orbit shrinks due to the hydrodynamical instability, the amplitude and the luminosity of gravitational waves gradually rise. When two stars of the binary come into contact, they become the maximum, and after that, they gradually fade away. Since the merged object becomes an ellipsoid in the final state and radiation reaction of gravitational waves is not included in this simulation, the wave form will settle down to a stationary one.

Before closing the section, we notice that evolution of the merged object and gravitational waves from it considerably depend on the velocity field of pre-merging state of binary: In the case where each star of binary does not have spin such as the irrotational Roche-Riemann

binary which is regarded as one of the most realistic situations for BNS [23], we have learned from numerical simulations that the large spiral arm is not formed [16) 24)]. Also, when radiation reaction of gravitational waves is included and as a result, pre-merging binary has an approaching velocity, the merged object radially oscillates and second and third peaks of the gravitational wave luminosity, which in the present result do not appear, can be seen [16) 8) 24)]. Thus, we should keep in mind that the present results on the evolution of merged object and gravitational waves from it are inherent for evolution of dynamically unstable corotating binary without radiation reaction.

§5. Summary

In this paper, we have shown numerical results of the hydrodynamical stability of corotating binary in equilibrium states in the 1PN approximation of general relativity. We found that the hydrodynamical instability sets in near the energy and/or angular momentum minima along the equilibrium sequence. This means that we may approximately determine the location of the ISCO from the energy and/or angular momentum minima along sequences for corotating binary.

As shown in previous papers, the angular velocity at those minima changes with the first GR correction approximately as [10) 11)]

$$\Omega = \Omega_{\rm N}\left(1 + C_{\rm PN}\frac{GM_*}{a_* c^2}\right), \tag{5·1}$$

where $\Omega_{\rm N}$ is the angular velocity at the minima for the Newtonian case and $C_{\rm PN}$ is a constant ~ 1.1 for $\Gamma = 3$ and ~ 2.5 for $\Gamma = 2$. For the polytropic EOS of $\Gamma = 3$ [10)] and 2 [11)],

$$\Omega_{\rm N} \simeq (0.267 \pm 0.002)\sqrt{\frac{GM}{a_0^3}} \quad \text{for } \Gamma = 3, \tag{5·2}$$

$$\simeq (0.297 \pm 0.002)\sqrt{\frac{GM}{a_0^3}} \quad \text{for } \Gamma = 2, \tag{5·3}$$

and the frequency of gravitational waves is calculated as

$$f_{\rm N} \equiv \frac{\Omega_{\rm N}}{\pi} \simeq 630\left(\frac{M}{1.4M_\odot}\right)^{1/2}\left(\frac{15{\rm km}}{a_0}\right)^{3/2} {\rm Hz} \quad \text{for } \Gamma = 3, \tag{5·4}$$

$$\simeq 700\left(\frac{M}{1.4M_\odot}\right)^{1/2}\left(\frac{15{\rm km}}{a_0}\right)^{3/2} {\rm Hz} \quad \text{for } \Gamma = 2, \tag{5·5}$$

where M and a_0 denote the Newtonian mass and radius of each star of binary, respectively. Since the EOS of NS has the adiabatic index of $2 \sim 3$, $f_{\rm N}$ may be approximated by

$$f_{\rm N} \simeq 600 - 700 \left(\frac{M}{1.4 M_\odot} \right)^{1/2} \left(\frac{15{\rm km}}{a_0} \right)^{3/2} {\rm Hz}. \qquad (5{\cdot}6)$$

Thus, in the case of corotating binary, the frequency of gravitational waves at the ISCO for a realistic BNS of radius 10$\sim$15km(i.e., $C_{\rm s} = 0.14 \sim 0.2$) will become about $150 \sim 300$Hz higher due to the 1PN correction of general relativity.

We performed numerical simulations only including the 1PN correction, i.e., the lowest order GR correction, in this paper, but it is not sufficient in order to obtain the ISCO for realistic BNS's accurately because BNS's are highly GR objects($C_{\rm s} \sim 0.2$). We need to take into account the fully GR term to obtain an accurate result. We, however, emphasize that the conclusion in this paper will hold for binaries of small compactness(say $C_{\rm s} \lesssim 0.05$). This means that when we perform fully GR simulation, the numerical code must reproduce the present result. Thus, the present paper will be a useful guideline in checking fully GR calculations.

Acknowledgments

Numerical computations were mainly performed on FACOM VX4 in data processing center of National Astronomical Observatory in Japan. This work was in part supported by a Grant-in-Aid of Ministry of Education, Culture, Science and Sports (08NP0801, 08237210 and 09740336).

References

[1] A. Abramovici, et al. Science **256**(1992), 325.

[2] C. Bradaschia, et al. Nucl. Instrum. and Methods **A289**(1990), 518.

[3] J. Hough, in *Proceedings of the Sixth Marcel Grossmann Meeting*, edited by H. Sato and T. Nakamura (World Scientific, Singapore, 1992), p.192.

[4] K. Kuroda et al. in *Proceedings of the international conference on gravitational waves: Sources and Detectors*, edited by I. Ciufolini and F. Fidecard(World Scientific, 1997), p.100.

[5] C. Cutler and É. É. Flanagan, Phys. Rev. D **49**(1994), 2658.
E. Poisson and C. M. Will, Phys. Rev. D **52**(1995), 848.

[6] L. Blanchet, T. Damour, B. R. Iyer, C. M. Will and A. G. Wiseman, Phys. Rev. Lett. **74**(1995), 3515.

L. E. Kidder, Phys. Rev. D **52**(1995), 821.
L. Blanchet, Phys. Rev. D **54**(1996), 1417.
[7] L. Lindblom, Astrophys. J. **398**(1992), 569.
[8] X. Zunge, J. M. Centrella, and S. L. W. Mcmillan, Phys. Rev. D **50** (1994), 6247; **54**(1996), 7261.
[9] D. Lai, F. A. Rasio, and S. L. Shapiro(LRS), Astrophys. J. **420** (1994), 811.
[10] M. Shibata, Prog. Theor. Phys. **96**(1996), 317: Note that there were two careless typewriting mistakes in this paper. (1) numerical values in the third column of Table II(i.e., $r_{\rm crit}/a_*$) are incorrect. The correct values are simply obtained by dividing them by $1.4^{1/5}$; (2) what is shown in vertical axis in fig.4 is $\Omega_{\rm crit}/(M_*/(2a_*)^3)^{1/2}$ not $\Omega_{\rm crit}a_*^{3/2}(M_*/2)^{-1/2}$.
[11] M. Shibata, Phys. Rev. D **55**(1997), 6019.
[12] L. Blanchet, T. Damour, and G. Schäfer, Mon. Not. R. Astro. Soc. **242** (1990), 289.
[13] For example, H. Asada, M. Shibata, and T. Futamase, Prog. Theor. Phys. **96**(1996), 81. See also references cited therein.
[14] K. Oohara and T. Nakamura, Prog. Theor. Phys. **88**(1992), 307.
[15] K. Oohara and T. Nakamura, Prog. Theor. Phys. **82**(1989), 535; **82**(1989), 1066; **83**(1990), 906;**86**(1991), 73.
[16] M. Shibata, T. Nakamura, and K. Oohara, Prog. Theor. Phys. **88**(1992), 1079.
[17] M. Shibata, Phys. Rev. D **55**(1997), 2002.
[18] For example, S. L. Shapiro & S. A. Teukolsky, *Black Holes, White Dwarfs, and Neutron Stars* (New York, Wiley, 1983).
[19] F. A. Rasio and S. L. Shapiro, Astrophys. J. **432**(1994), 242.
[20] K. C. B. New and J. E. Tohline, gr-qc/9703013.
[21] M. Shibata and K. Taniguchi, Phys. Rev. D **56**(1997) to be published.
[22] É. É. Flanagan, Preprint gr-qc/9706045:
K. S. Thorne, Preprint gr-qc/9706057.
[23] C. S. Kochanek, Astrophys. J. **398**(1992), 234.
L. Bildsten and C. Cutler, Astrophys. J. **400**(1992), 175.
[24] M. Ruffert, H.-T. Janka and G. Schäfer, Astro. and Astrophysics **311**(1996), 532;
M. Ruffert, M. Rampp and H.-T. Janka, Astro. and Astrophysics, **321**(1997), 991.

Figure captions

Fig.1 The energy(a) and the angular momentum(b) of corotating binary in equilibrium states

as a function of the orbital separation r_g/a_* for the 1PN case of $r_0 = 40R_s$(filled circles) and the Newtonian case(open circles). The energy and the angular momentum are shown in units of GM_*^2/a_* and $G^{1/2}M_*^{3/2}a_*^{1/2}$, respectively.

Fig.2 Normalized moment $I_{RR}/(M_*a_*^2)$ as a function of time for the Newtonian case(a) and the 1PN case of $C_{\rm s} \simeq 0.033$(b). Units of time is $4\pi\sqrt{a_*^3/GM_*}$. Solid, dotted, dashed and dotted-dashed lines are for models N5(PN5), N6(PN6), N7(PN7), and N8(PN8), respectively.

Fig.3 The angular momentum as a function of time. Units of the angular momentum and the time are $G^{1/2}M_*^{3/2}a_*^{1/2}$ and $4\pi\sqrt{a_*^3/GM_*}$, respectively. Solid, dotted, dashed and dotted-dashed lines are for models N5(PN5), N6(PN6), N7(PN7), and N8(PN8), respectively.

Fig.4 The same as fig.3, but for the maximum density. Units of the density is $M_*(4\pi a_*^3/3)^{-1}$.

Fig.5 Time evolution of the density(ρ) profile in the equatorial plane for model N7. x and y-axes are shown in units of $a_*(= a_0)$. Note that outermost grid is placed at 4.09 in this units, and the orbital rotation is counterclockwise. Density contours(solid lines) are spaced with intervals of $\rho_{\rm max,0}/10$, where $\rho_{\rm max,0}$ is the maximum density at the initial state. Dotted lines denote contour of $\rho_{\rm max,0}/100$.

Fig.6 The same as fig.5, but for ρ_* of model PN7.

Fig.7 The same as fig.5, but for model N5.

Fig.8 The same as fig.5, but for ρ_* of model PN5.

Fig.9 Wave forms $r_o h_+$(a) and $r_o h_\times$(b), and the luminosity(c) of gravitational waves for models PN5(solid lines) and N5(dotted lines). Units of the amplitude of $r_o h_+$ and $r_o h_\times$, the luminosity, and time are $G^2M_*^2/c^4a_*$, $c^5/G(GM_*/a_*c^2)^5$ and $4\pi\sqrt{a_*^3/GM_*}$, respectively.

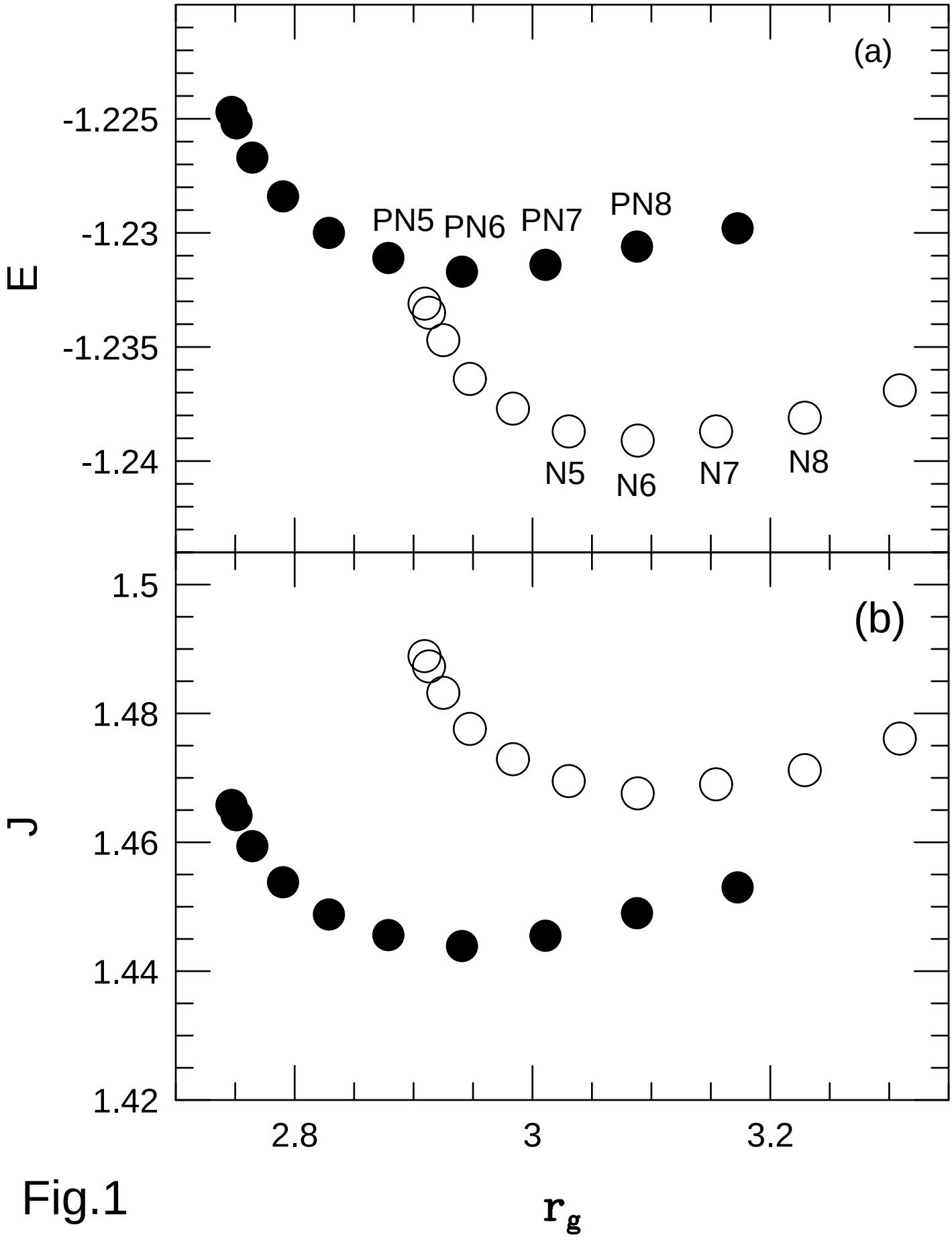
(a)
-1.225
-1.23
-1.235
-1.24
E
PN5
PN6
PN7
PN8
N5
N6
N7
N8
(b)
1.5
1.48
1.46
1.44
1.42
J
2.8
3
3.2
r_g

Fig.1

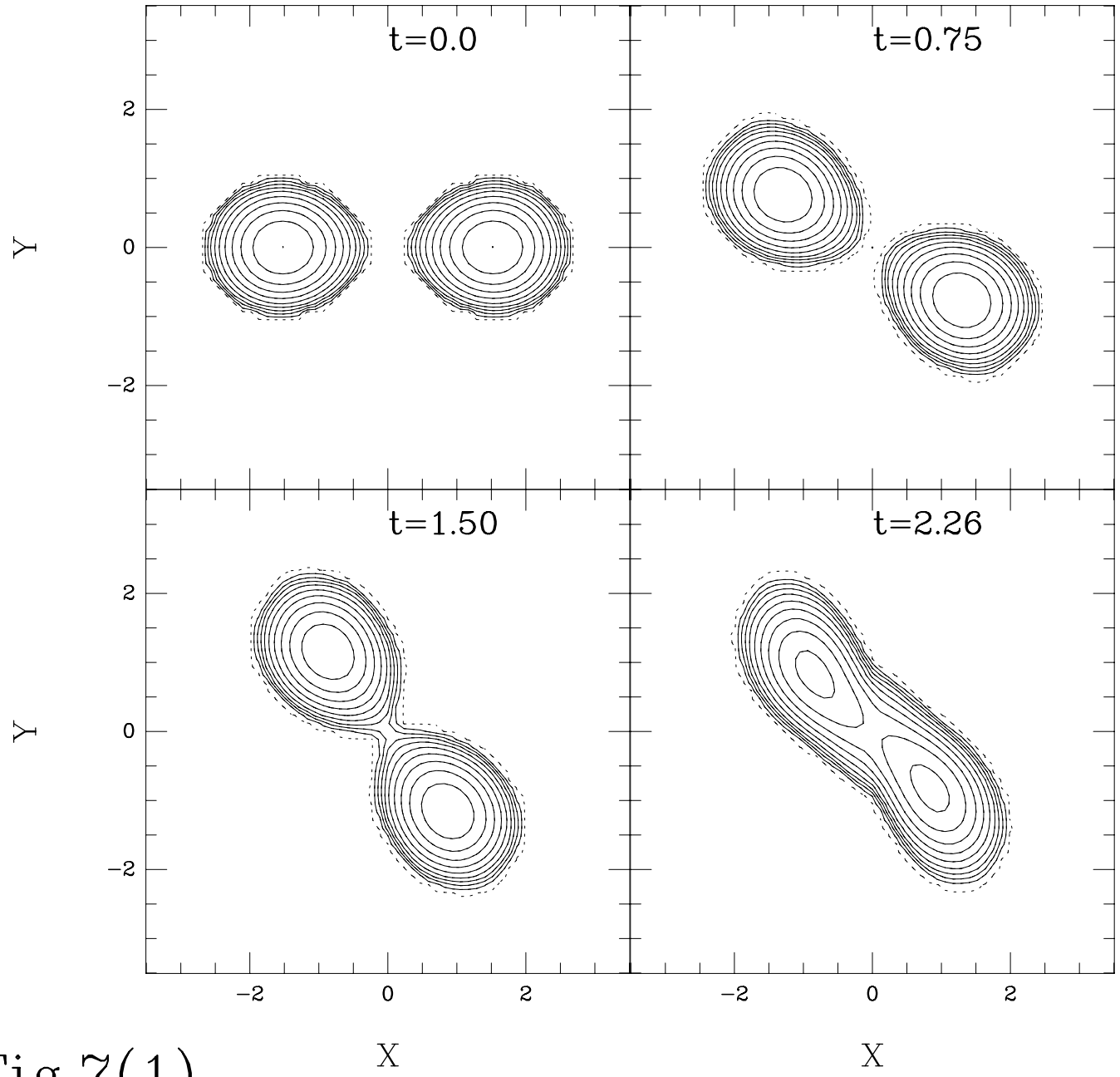

Fig.7(1)

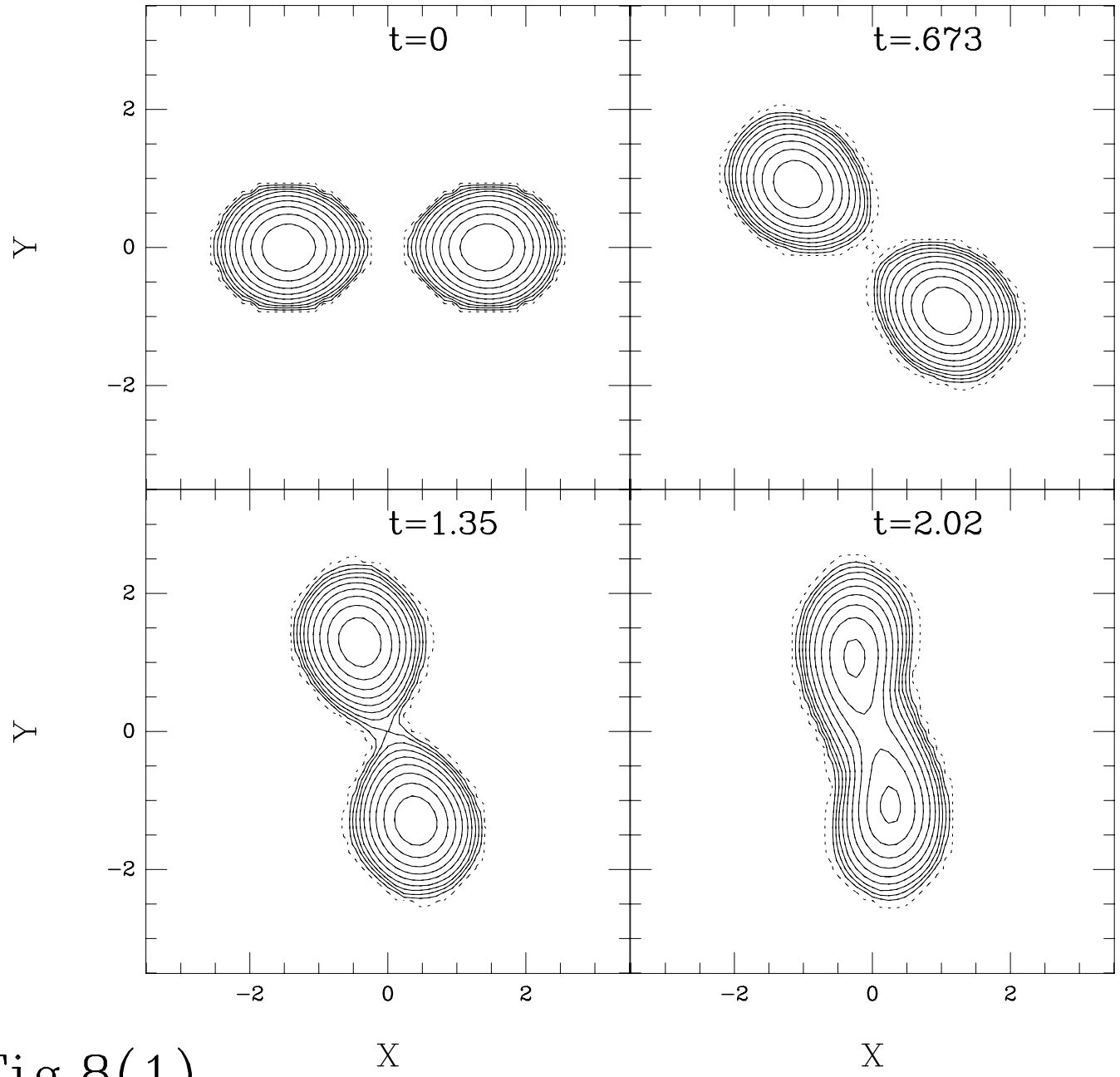

Fig.8(1)

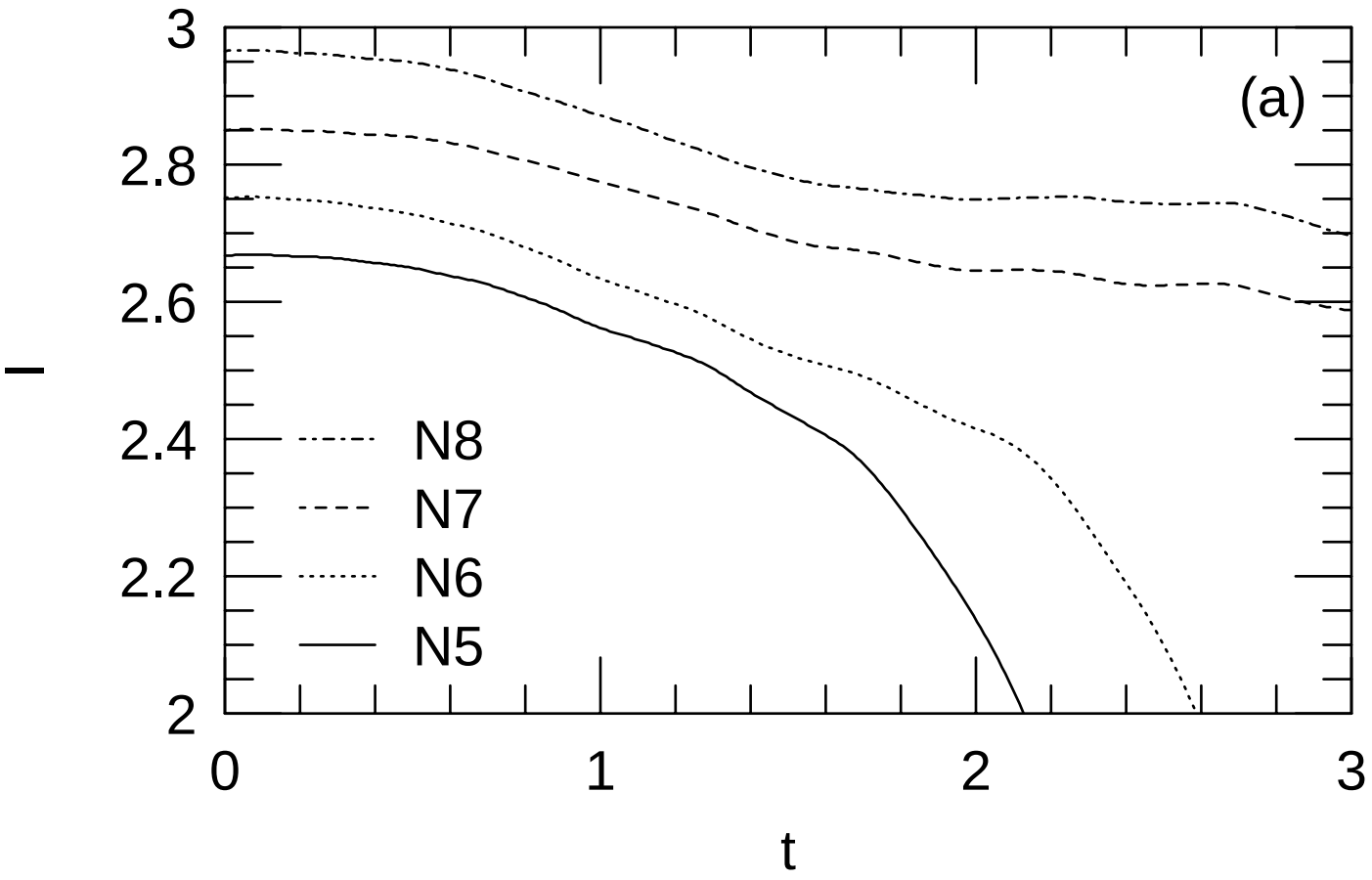
(a)
N8
N7
N6
N5
3
2.8
2.6
2.4
2.2
2
0
1
2
3
t

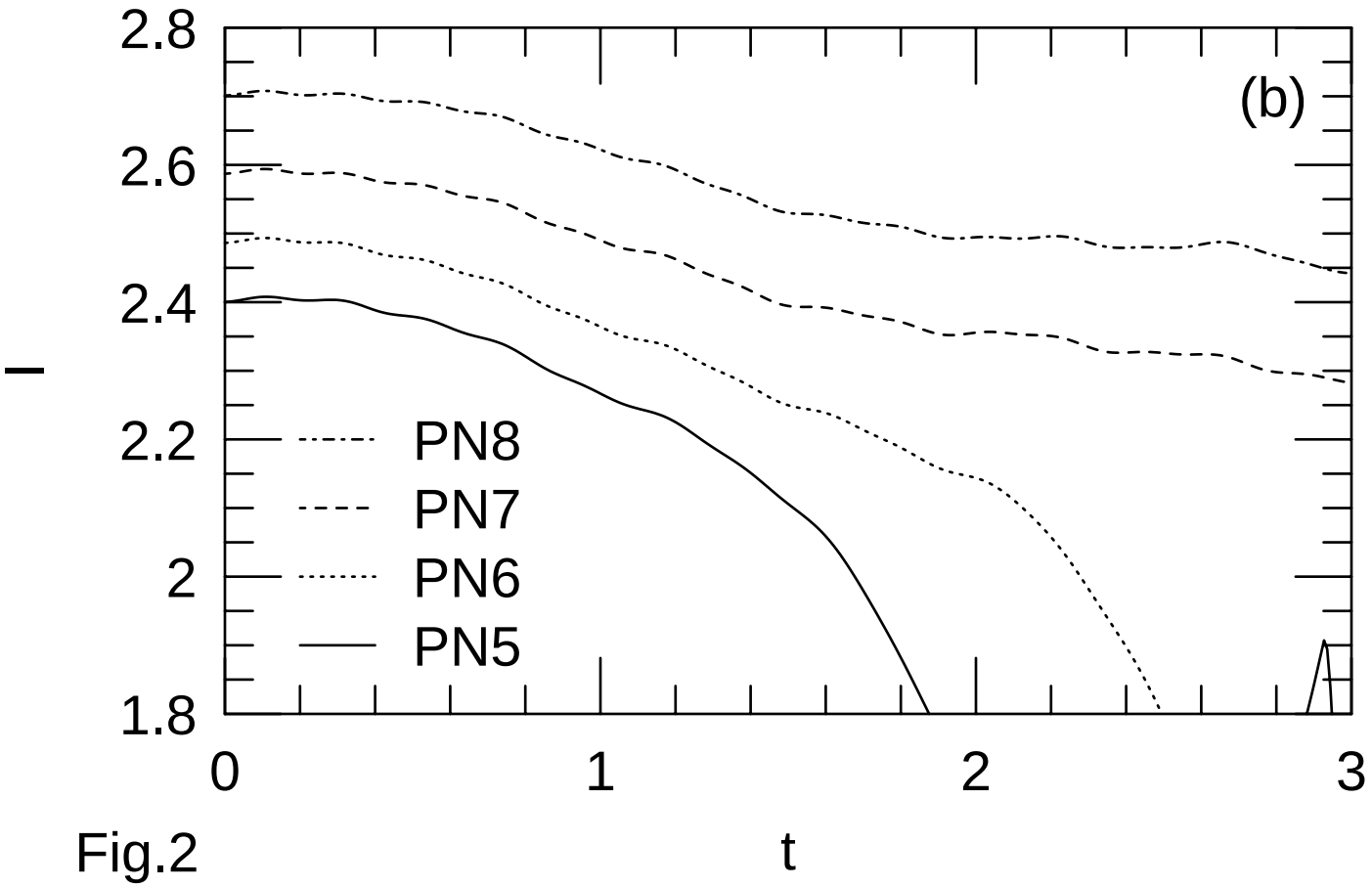
(b)
PN8
PN7
PN6
PN5
2.8
2.6
2.4
2.2
2
1.8
0
1
2
3
t

Fig.2

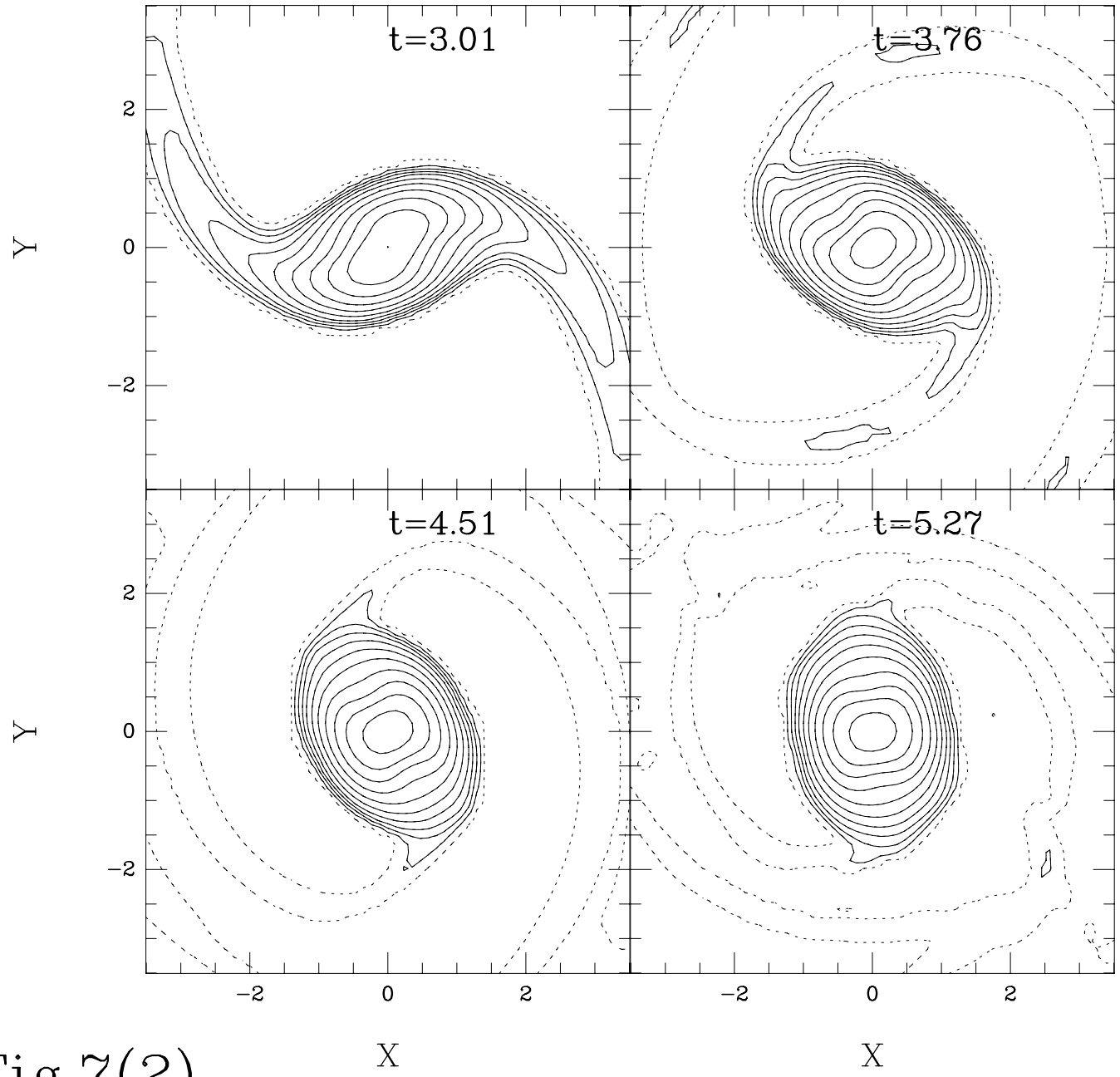

Fig.7(2)

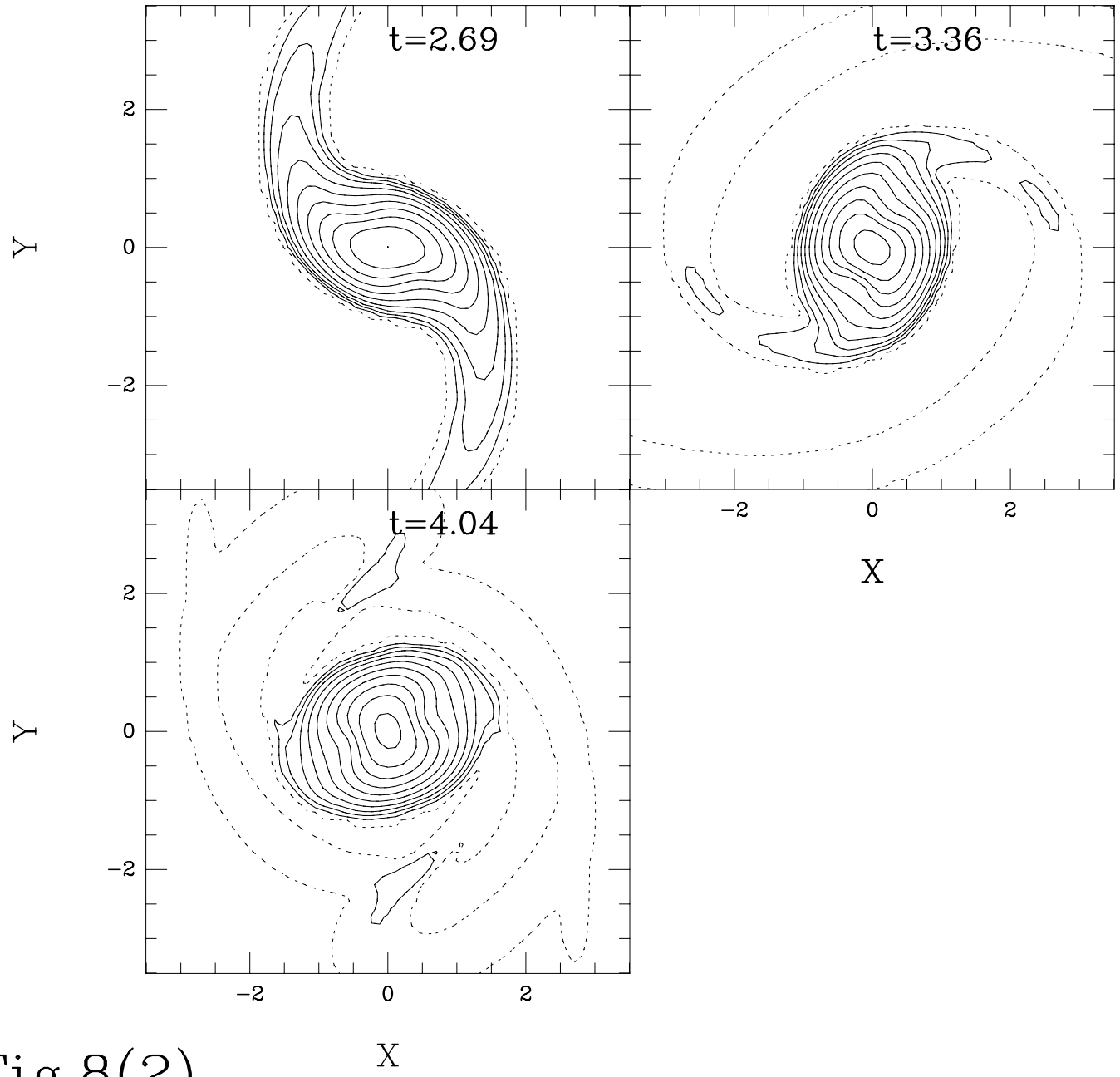

Fig.8(2)

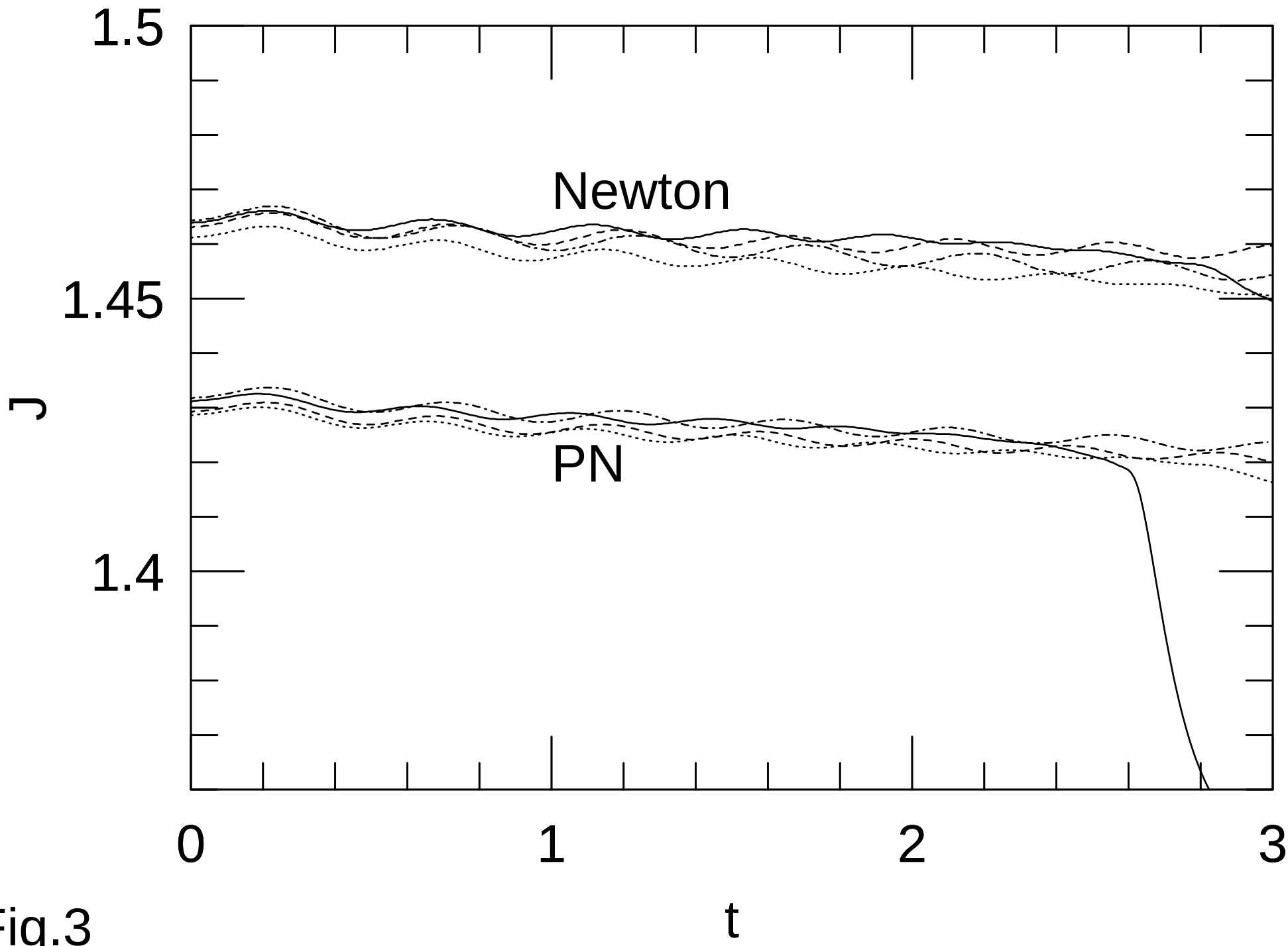

Fig.3

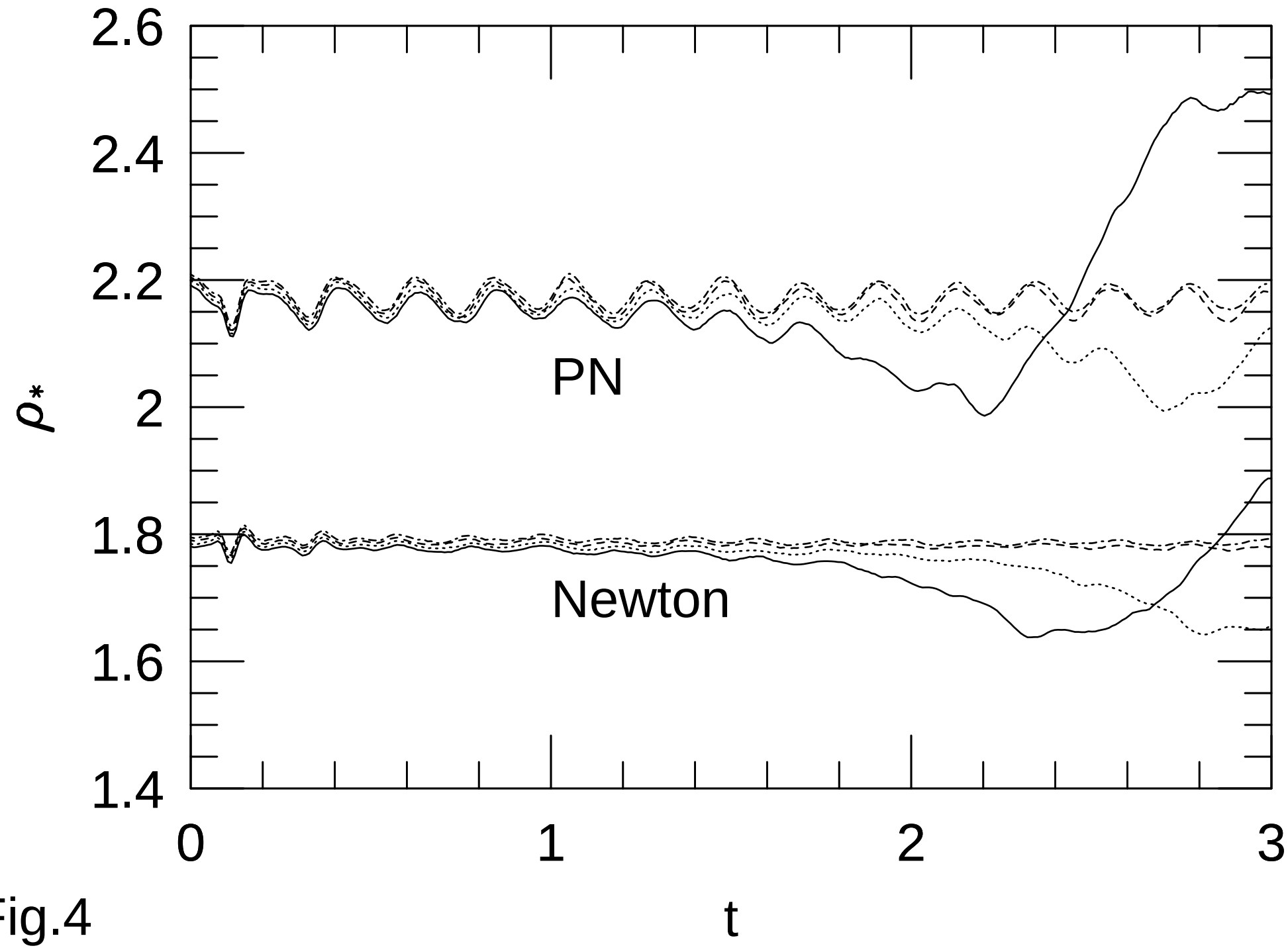

Fig.4

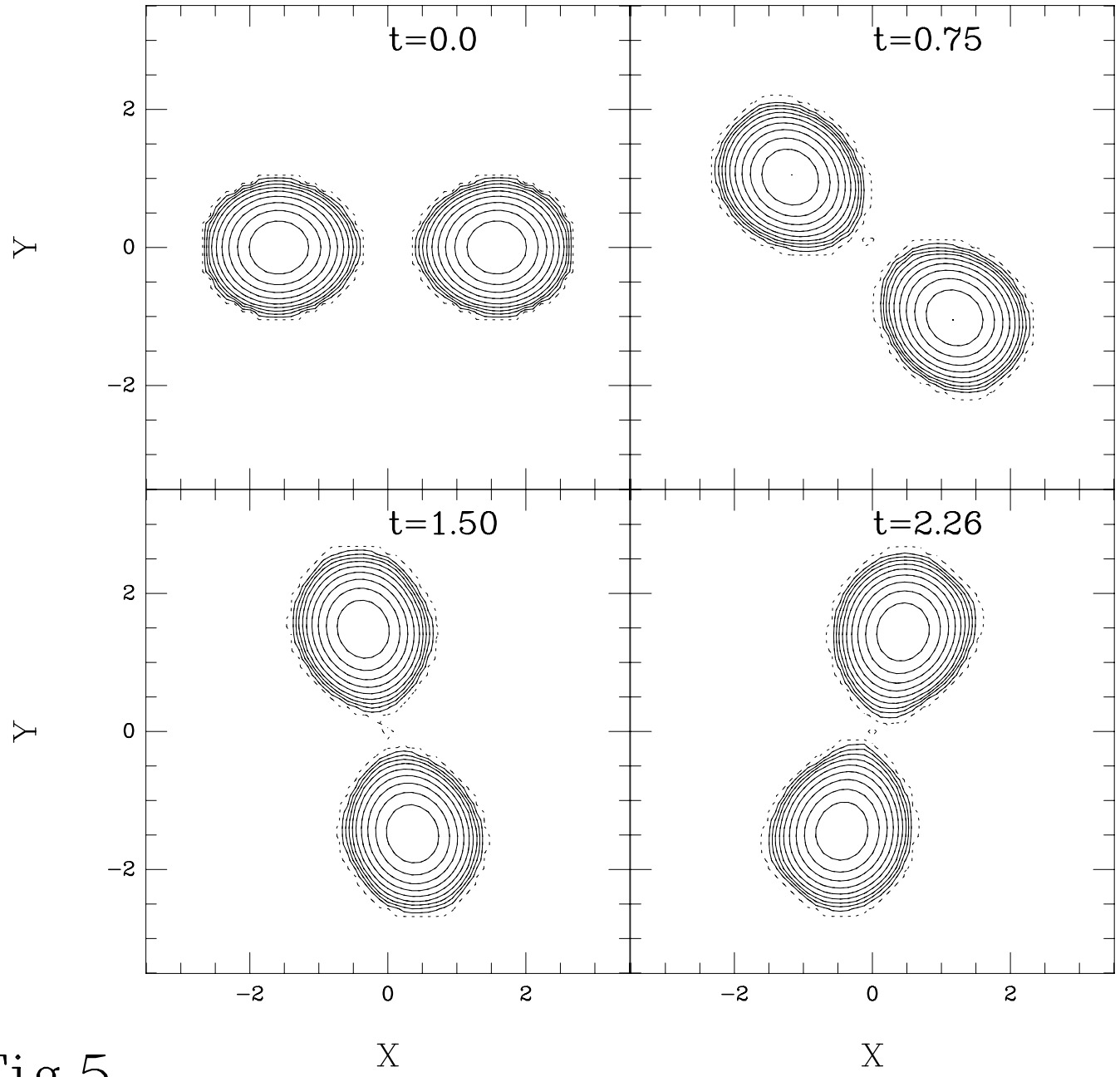

Fig.5

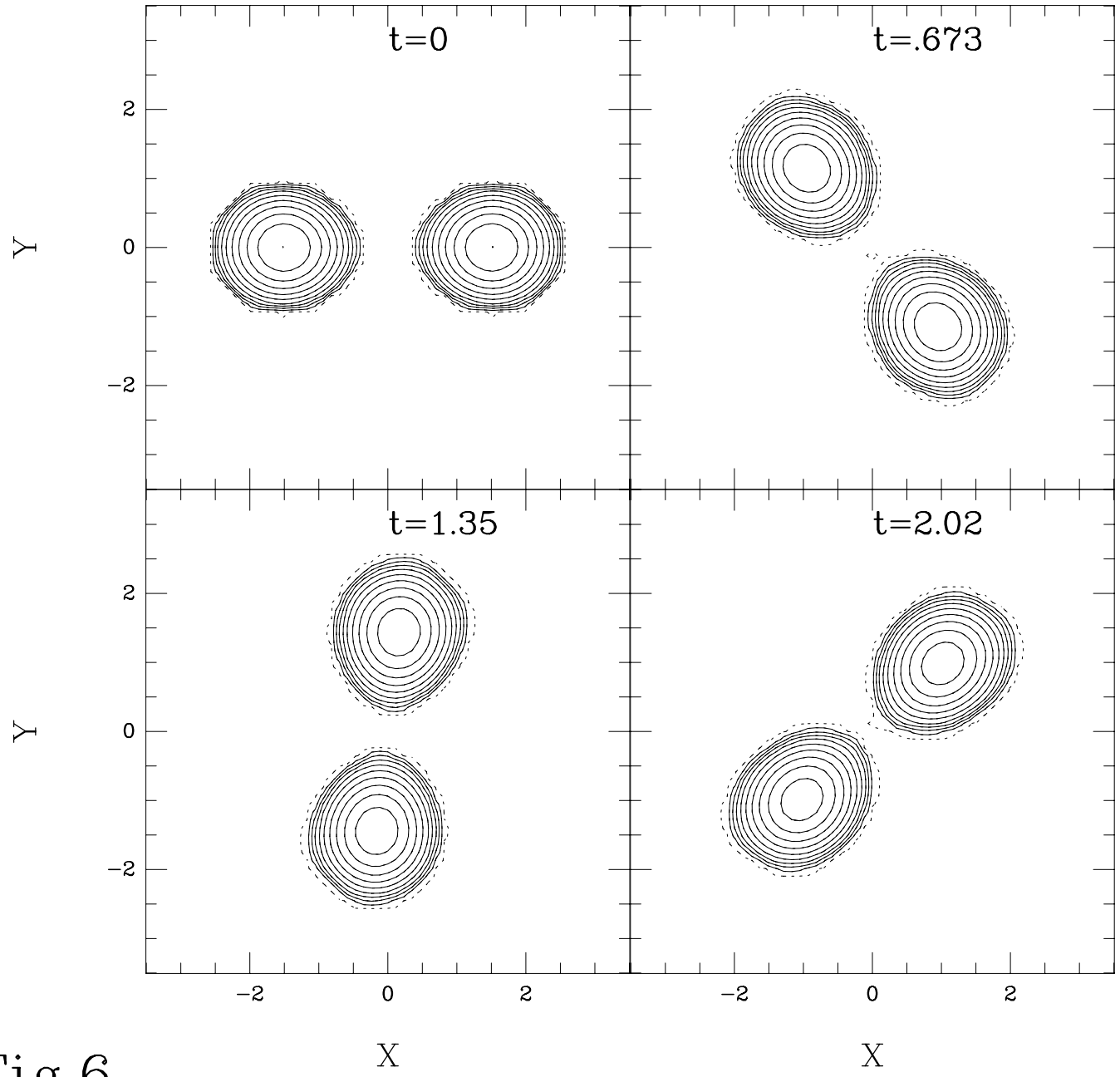

Fig.6

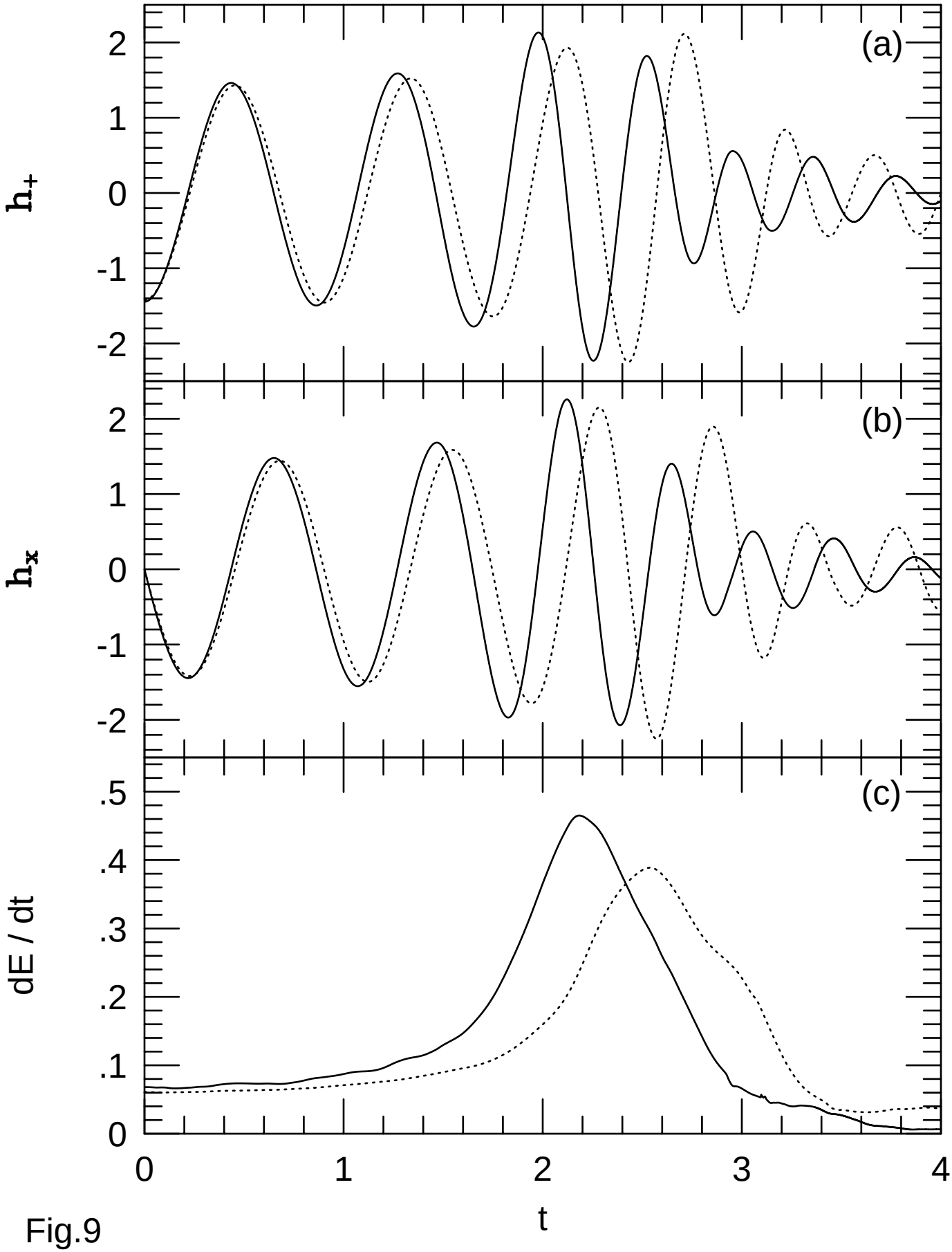

Fig.9